Land Vehicle Dynamics-Aided Inertial Navigation

J-H. WANG
Applanix, a Trimble Company
Canada

Y. GAO
The University of Calgary

The major challenge of using low-cost micro-electro-mechanical-system (MEMS) inertial navigation system (INS) is the rapid navigation error drift when the aiding sensors are unavailable. A self-contained dynamics-aided error correction method is developed to overcome this problem. Additional measurements are generated to update the navigation filter and control the navigation error based on the knowledge of land vehicle dynamics. The contribution of the proposed dynamics-aided method to INS/GPS navigation during long GPS outages has been demonstrated through field tests.

Manauscript received December 4, 2007; revised October 2, 2008; released for publication March 20, 2009.

IEEE Log No. T-AES/46/4/938747.

Refereeing of this contribution was handled by D. Aloi.

Authors' addresses: J-H. Wang, 85 Leek Crescent, Richmond Hill, ON, Canada L4B 3B3, E-mail: (jhwang@applanix.com); Y. Gao, The University of Calgary, 2500 University Drive, N.W., Calgary, Alberta, T2N 1N4.

I. INTRODUCTION

Inertial navigation system (INS) is a dead-reckoning navigation system which determines the attitude, velocity, and position of a moving body from the knowledge of the previous states and the measurements of the motion. Inertial navigation error will accumulate with time due to the integration of measurement errors. Aided INS with other enabling sensors has been widely used in applications. In some applications, however, the aiding sensors might not always be available. For example, the Global Positioning Systems (GPS) aided INS will lose aiding data when satellite signals are blocked or jammed. During this unaided or stand-alone inertial navigation, the navigation filter will predict and correct the navigation errors based on the last inertial sensor error estimates and the error dynamics model. The filter error prediction accuracy however is highly dependent on the inertial sensor quality. For high performance INS, the sensor errors can be accurately estimated and compensated for by a well-designed Kalman filter [1–3]. But for low-cost micro-electro-mechanical-system (MEMS)–based INS with large bias variation and random error, both of which are difficult to characterize, the navigation errors cannot be predicted by the Kalman filter accurately and will drift rapidly [4–6].

A number of approaches have been proposed to reduce the stand-alone INS error drift by developing special error prediction techniques and aiding methods from vehicle dynamics knowledge. For instance, neural networks and neuro-fuzzy models have been proposed to predict INS drift errors based on an input/output pattern memorized during a training or learning process [7–9]. To maintain good performance of the neuro-fuzzy prediction, however, the training data must cover all the input and output data ranges, and the neuro-fuzzy model should be retrained frequently to deal with minor changes in the operating environmental conditions [10]. This requires a lot of data computation, and therefore the method is not applicable to real-time applications. In addition, for a low-grade INS with relatively high instrument bias, noise, and random error, its sensor errors are highly sensitive to operational environments. As a result, the input/output patterns will change dynamically and will be unlikely to repeat the environments as given by the used training data. The use of a pretrained neuro-fuzzy model to predict navigation errors therefore presents a great challenge to the method.

For land vehicle applications the constraints of the vehicle motion can be used to reduce INS error drift. Zero velocity updates (ZUPTs) are the most commonly used techniques to provide effective INS error control if the vehicle sometimes remains

stationary, for instance if it stops before the stop sign [11]. In addition, Brandt and Gardner (1998), Dissanayake et al. (2001) and Shin (2005) have applied the nonholonomic constraints that govern the motion of a vehicle on a surface to bind the mechanization errors [12–14]. Collin et al. (2001), Ojeda and Borenstein (2002), and Wang and Gao (2004) have used the complementary motion detection characteristics of the accelerometers and gyroscopes to keep the tilt estimation bounded [15–17]. The idea behind it is to use the accelerometer-derived tilt angle to update the attitude when the vehicle is stationary or moving at a constant speed. Among these methods, however, only ZUPTs can provide direct error control of the forward velocity of the vehicle but they are not always frequently available. For low-cost MEMS INS with large instrument errors, the control of an INS navigation error using these methods is insufficient especially during long GPS outages.

This paper develops additional measurements derived from land vehicle dynamics knowledge to control the stand-alone INS navigation error by modifying the previous developments in [18]. We derive roll data and forward velocity from INS measurements under certain dynamics of a land vehicle including straight-line and cornering motions. Together with ZUPTs, stationary heading constraint, and tilt data, the dynamics aiding data can now be available not only when the vehicle is stationary but also when it is moving. To apply these dynamics-dependent aiding data properly, the vehicle dynamics should be first identified, and in this paper this is accomplished by a fuzzy expert system. The dynamics aiding data are then used to update the navigation Kalman filter when the primary aiding sources such as GPS becomes unavailable due to signal blockages. This dynamics-aiding method has been applied to a MEMS-based INS/GPS integrated system, and its navigation performance to bridge GPS outage has been evaluated by the field test. The test results have shown that the dynamic-aiding method can improve the positioning accuracy from the 100 m level of non-dynamics-aided INS to around 15 m with 3 min GPS outages.

The remainder of this paper is organized as follows. First, we derive the dynamic-dependent observables from the land vehicle motion model. Next we present the design of a fuzzy expert system used for land vehicle dynamics identification. We then present the design of a dead-reckoning Kalman filter and analyze the error characteristic of the dynamic-derived measurements. Finally, the experimental results are described to demonstrate the benefit of the dynamics-aided method, and the paper ends with our conclusions.

II. VEHICLE DYNAMICS-DERIVED OBSERVABLES

A. Land Vehicle Motion Model

In this paper, the land vehicle motion model developed by Brandt and Gardner (1998) is used for INS navigation computation [12]. This model is derived from the traditional INS navigation equations with the nonholonomic constraints, i.e., no motion along the transverse direction and the direction normal to the road surface for a land vehicle. This model also assumes that Earth rotation is negligible and that the gravity vector is constant. The land vehicle motion model is particularly applied for low-grade inertial systems to improve the navigator performance in the presence of high sensor noise and bias variation. The land vehicle motion model is shown from (1) to (9), and the derivation can be found in Brandt and Gardner or Dissanayake, et al. [12, 13].

$$\dot{V}_f = A_{Bx} - g\sin\theta \tag{1}$$

$$V_f\omega_{Bz} = A_{By} + g\sin\phi\cos\theta \tag{2}$$

$$V_f\omega_{By} = -A_{Bz} - g\cos\phi\cos\theta \tag{3}$$

$$\dot{\phi} = \omega_{Bx} + \sin\phi\tan\theta\omega_{By} + \cos\phi\tan\theta\omega_{Bz} \tag{4}$$

$$\dot{\theta} = \cos\phi\omega_{By} - \sin\phi\omega_{Bz} \tag{5}$$

$$\dot{\psi} = \frac{\sin\phi}{\cos\theta}\omega_{By} + \frac{\cos\phi}{\cos\theta}\omega_{Bz} \tag{6}$$

$$\dot{P}_{Nn} = V_f\cos\theta\cos\psi \tag{7}$$

$$\dot{P}_{Ne} = V_f\cos\theta\sin\psi \tag{8}$$

$$\dot{P}_{Nd} = V_f\sin\theta \tag{9}$$

where $(\dot{\cdot})$ denotes the time derivative of $(\cdot)$. The subscript N indicates the navigation frame represented by three orthogonal axes in local north (n), east (e) and down (d) directions; the subscript B indicates the body frame represented by three orthogonal axes in the forward (x), transverse (y), and down (z) directions of the vehicle; $[P_{Nn}, P_{Ne}, P_{Nd}]^T$ is the position of the vehicle in the navigation frame; V_f is the speed of the vehicle; $[\phi, \theta, \psi]^T$ is the attitude of the vehicle expressed by three Euler angles, namely Roll (ϕ), Pitch (θ), and Yaw (ψ), which are the rotation angles about the x, y, and z axes, respectively; $[A_{Bx}, A_{By}, A_{Bz}]^T$ is the measured acceleration in the body frame; $[\omega_{Bx}, \omega_{By}, \omega_{Bz}]^T$ is the measured angular velocity in the body frame; g is the gravitational constant.

Equations (1) and (2) indicate the following.

1) The forward velocity of the vehicle can be directly computed from A_{By}, ϕ, and θ if the angular velocities ω_{Bz} are significantly large, i.e., when the vehicle is turning.

2) The roll and pitch can be directly computed under special dynamics, e.g., when the vehicle is static, roll and pitch can be directly computed from A_{Bx} and A_{By} and when the vehicle is moving straight in which ω_{Bz} are significantly small, roll can be directly computed from A_{By} and θ.

Thus, it is possible, under some specific vehicle dynamics, to directly estimate some navigation states such as tilt angles and the velocity of a land vehicle without using external sensors. These dynamics-derived estimates can be used to update the INS Kalman filter for navigation error control. The following section will present the development of the dynamics-aided measurements according to the dynamics: stationary, straight-line motion, and cornering motion.

B. Stationary Dynamics-Derived Observables

The first direct measurement during the stationary periods is the well-known ZUPT. ZUPT provides a very accurate velocity observation to correct velocity error when the vehicle is static. ZUPT can also correct the position and attitude error based on the correlation between the velocity, position, and attitude error in INS error dynamics. However, for MEMS-based inertial measurement unit (IMU) with large bias variation and random noise, the statistical observability is weak, and the position and attitude error corrections from ZUPT are not accurate.

An alternative to correct attitude error when a vehicle is stationary is to use accelerometer measurements. Accelerometer measurements can be used to directly derive accurate pitch and roll angles if the vehicle is static. Measuring only the local gravity field under this condition, the accelerometer outputs can be used to determine the vehicle pitch and roll angles using (1) and (2) as follows:

$$\theta = \sin^{-1}\left(\frac{A_{Bx}}{g}\right) \tag{10}$$

$$\phi = \sin^{-1}\left(\frac{-A_{By}}{\sqrt{g^2 - A_{Bx}^2}}\right). \tag{11}$$

According to (10) and (11), no integration step in time is required, and the accuracy of the tilt estimate is mainly governed by the accelerometer measurement error such as bias and noise. Using the perturbation technique, we can derive the following equations to describe the relationship between the accelerometer measurement error and the tilt error.

$$\delta\theta = \frac{1}{\sqrt{g^2 - A_{Bx}^2}}\delta A_{Bx} \tag{12}$$

$$\begin{aligned}\delta\phi &= \frac{\sqrt{g^2 - A_{Bx}^2 - A_{By}^2}}{\sqrt{g^2 - A_{Bx}^2}}\left(\frac{-\delta A_{By}}{\sqrt{g^2 - A_{Bx}^2}} - \frac{A_{Bx}A_{By}\delta A_{Bx}}{(g^2 - A_{Bx}^2)^{3/2}}\right)\\ &= \sqrt{g^2 - A_{Bx}^2 - A_{By}^2}\left(\frac{-\delta A_{By}}{(g^2 - A_{Bx}^2)} - \frac{A_{Bx}A_{By}\delta A_{Bx}}{(g^2 - A_{Bx}^2)^2}\right)\\ &\cong -\frac{\sqrt{g^2 - A_{Bx}^2 - A_{By}^2}}{(g^2 - A_{Bx}^2)}\delta A_{By}\end{aligned} \tag{13}$$

where $\delta\theta$ and $\delta\phi$ are pitch and roll errors, and δA_{Bx} and δA_{By} are the x-axis and y-axis accelerometer measurement errors, respectively.

For land vehicle applications where the tilt angle is usually small and the stationary A_{Bx} and A_{By} are relatively much smaller than the gravity, a 1 mg unidentified accelerometer bias will lead to a tilt error of about 0.057 deg. Accelerometer noise effects can be reduced by averaging the tilt estimates over the stationary periods. Compared with the gyro-derived tilt with large drift errors, the accelerometer-derived tilt is relatively accurate and able to provide direct correction of the tilt error.

Another observation available during the stationary periods is the constant heading constraint which can stop the drift of the heading error. Since the vehicle is not moving, the heading of the vehicle can be considered unchanged and can be modeled by the following equation:

$$\psi(t_s) = \psi(t_s - 1) \tag{14}$$

where t_s denotes the sampling time during the stationary periods.

The last benefit from the stationary mode is the availability of the gyro bias estimate. For automotive-grade and consumer-grade IMUs, the stationary outputs of gyroscopes themselves can be considered as measurement biases [19]. This is because the Earth's rotation is at the sensor noise level for automotive-grade MEMS IMUs, and thus the true angular rate of the body frame during the stationary periods can be assumed to be zero. By averaging all gyro measurements during the stationary periods, we can remove the noise effects and use this average value as the current gyro bias estimate.

C. Straight-Line Dynamics-Derived Observables

When a vehicle is moving straight, no significant motion acceleration along the transverse direction exists. Thus, primarily the y-axis accelerometer measurement, which contains the local gravity field, can be used to determine the approximate roll angle based on (3) with $\omega_{Bz} = 0$. Although the approximation errors induced by sideslips or vibrations may exist, they can be mostly reduced by moving the average over time. Therefore, when the vehicle

is moving straight, the accelerometer-derived roll still can be used as a direct roll update to reduce the drift error of the gyro-derived tilt. Similar to the stationary tilt estimates, the accuracy of the accelerometer-derived roll depends on the accuracy of the estimated y-axis accelerometer bias.

D. Cornering Dynamics-Derived Observables

In addition to ZUPTs, the cornering motion with strong dynamics in transverse acceleration and yawing provides another occurrence for direct estimation of the vehicle velocity. Rearranging (2), the forward velocity of the vehicle can be directly estimated as follows:

$$V_f = \frac{1}{\omega_{Bz}}(A_{By} + g\sin\phi\cos\theta). \tag{15}$$

According to the above equation, the forward velocity is inversely proportional to the z-axis gyro measurement. Thus, the estimation of the forward velocity is not applicable if the signal-to-noise ratio of the z-axis gyro measurement is low. Only when the z-axis angular dynamics is significant, e.g., during the cornering motion, the estimation of the forward velocity becomes feasible. Using the perturbation technique, we can derive the following equation to describe the error budget of the forward velocity estimate:

$$\delta V_f = \frac{1}{\omega_{Bz}}(\delta A_{By} + g\cos\phi\cos\theta\delta\phi - g\sin\phi\sin\theta\delta\theta) - \frac{1}{\omega_{Bz}^2}(A_{By} + g\sin\phi\cos\theta)\delta\omega_{Bz}. \tag{16}$$

where δV_f and $\delta\omega_{Bz}$ are the errors of the forward velocity and the z-axis gyro measurement, respectively.

According to the above equation, the accuracy of the forward velocity estimate depends on the accuracy of the y-axis accelerometer measurement, the z-axis gyro measurement, and the tilt estimate. Since tilt angles are generally small during the cornering motion of a land vehicle and thus the term $\sin\phi\sin\theta$ in (16) becomes very small, the effect of the pitch error on the forward velocity estimate is negligible. In addition, because the accelerometer-derived roll is always used to update the roll estimate when the vehicle is stationary or moving straight, the accuracy of the roll estimate during cornering is mainly governed by the y-axis accelerometer error. Therefore, we can replace $\delta\phi$ in (16) with (13) and rewrite (16) as follows:

$$\begin{aligned}\delta V_f &= \frac{1}{\omega_{Bz}}\left(\delta A_{By} - g\cos\phi\cos\theta\frac{\sqrt{g^2 - A_{Bx}^2 - A_{By}^2}}{(g^2 - A_{Bx}^2)}\delta A_{By} - g\sin\phi\sin\theta\delta\theta\right) - \frac{1}{\omega_{Bz}^2}(A_{By} + g\sin\phi\cos\theta)\delta\omega_{Bz} \\ &\cong \frac{1}{\omega_{Bz}}\left(1 - g\cos\phi\cos\theta\frac{\sqrt{g^2 - A_{Bx}^2 - A_{By}^2}}{(g^2 - A_{Bx}^2)}\right)\delta A_{By} - \frac{1}{\omega_{Bz}^2}(A_{By} + g\sin\phi\cos\theta)\delta\omega_{Bz}.\end{aligned} \tag{17}$$

Based on (17), the accuracy of the forward velocity estimate is mainly determined by IMU measurement errors such as bias, noise of the y-axis accelerometer, and the z-axis gyro. In general, ω_{Bz} is large, and the tilt angles are small during the cornering motion of a land vehicle; thus the impact of δA_{By} and $\delta\omega_{Bz}$ on the velocity estimation error is diminished. For example, a typical cornering motion where A_{Bx} is 1.0 m/s^2, A_{By} is 1.5 m/s^2, ω_{Bz} is 15 deg/s, ϕ is 2 deg, and θ is 2 deg, 1 m/s^2 δA_{By} will cause 0.03026 m/s error in the velocity estimate, and 0.1 deg/s $\delta\omega_{Bz}$ will cause -0.0469 m/s error in the velocity estimate.

E. Summary

The vehicle dynamics-derived observations under different dynamics are summarized in Table I. We find that the stationary dynamics provides the most dynamics-derived observations for INS error estimation and correction including attitude error, velocity error, and gyro bias. During the straight-line motion, direct estimation of the roll angle is possible, and the roll error can be well bounded and controlled by the accelerometer measurements. When the vehicle makes a turn, a direct estimation of the forward velocity is available and the velocity error drift can be reduced. The accuracy of the dynamics-derived observations is mainly governed by the accelerometer and gyro biases. These biases might be removed by using the filter-estimated biases when the primary aiding sensor such as GPS is available. The drift-free dynamics-derived observations are more accurate than the stand-alone INS navigation states and can provide self-contained INS error correction.

III. VEHICLE DYNAMICS IDENTIFICATION

In order to implement the aforementioned dynamics-dependent aiding for INS error control, the vehicle dynamics such as stationary, straight-line motion, and cornering motion must be correctly identified. As inertial measurements such as acceleration and angular velocity strongly relate

TABLE I
Vehicle Dynamics-Derived Observations

	Direct Estimation of INS Navigation States and Sensor Errors				
Vehicle Dynamics	Pitch	Roll	Yaw	Forward Velocity	Gyro Bias
Stationary	$\theta = \sin^{-1}\left(\frac{A_{Bx}}{g}\right)$	$\phi = \sin^{-1}\left(\frac{-A_{By}}{\sqrt{g^2 - A_{Bx}^2}}\right)$	$\psi(t_s) = \psi(t_s - 1)$	$V_f = 0$	$b_{\omega_{Bx}} = \omega_{Bx}$ $b_{\omega_{By}} = \omega_{By}$ $b_{\omega_{Bz}} = \omega_{Bz}$
Straight-line Motion	N/A	$\phi = \sin^{-1}\left(\frac{-A_{By}}{\sqrt{g^2 - A_{Bx}^2}}\right)$	N/A	N/A	N/A
Cornering Motion	N/A	N/A	N/A	$V_f = \frac{A_{By} + g\sin\phi\cos\theta}{\omega_{Bz}}$	N/A

to vehicle dynamics, they can be used for vehicle dynamics identification through a reasoning or/and rule-based decision-making process. In real-life applications, however, these raw measurements are corrupted with noise and vibration effects especially for low-cost MEMS IMUs. Therefore, the identification system must be capable of dealing with the imprecision of inertial measurements as well. As fuzzy set theory provides a natural method for dealing with linguistic terms to effectively represent imprecise and ambiguous information, a fuzzy expert system that incorporates a fuzzy inference system and expert rules into its reasoning process and knowledge representation scheme has been applied in this paper for vehicle dynamics identification.

The fuzzy inference system is a computing framework to formulate the mapping from a given input to an output based on the concept of fuzzy set theory, fuzzy logic operators, if-then rules, and defuzzification. In a typical fuzzy inference system, the crisp inputs are first converted to the input fuzzy sets using the membership functions. Then the input fuzzy sets are mapped into a consequent fuzzy set based on the adopted fuzzy logic operators, if-then rules, and aggregation strategy. Finally, the consequent fuzzy set is converted into a scalar quantity as the system output using a defuzzification method. As the fundamentals of the fuzzy expert system can be found in many textbooks [20, 21], the following descriptions focus on the parameter and rule design of the fuzzy expert system for vehicle dynamics identification.

To consider both linear and angular dynamics, we define the input variables of the fuzzy inference system $J(t_k)$ and $W(t_k)$ as follows:

$$J(t_k) = \sum_{t_i = t_k - n}^{t_k} |A_{\text{norm}}(t_i) - A_{\text{norm}}(t_i - 1)| \tag{18}$$

$$W(t_k) = \sum_{t_i = t_k - n}^{t_k} |\omega_{\text{norm}}(t_i)| \tag{19}$$

where $A_{\text{norm}} = \sqrt{A_{Bx}^2 + A_{By}^2 + A_{Bz}^2}$ is the norm of the three-axis accelerations, $\omega_{\text{norm}} = \sqrt{\omega_{Bx}^2 + \omega_{By}^2}$ is the norm of the x-axis and y-axis angular velocities, t_k denotes the current discrete time, and n is the size of time window for statistical smoothing.

The first input variable $J(t_k)$ indicates the overall linear jerk dynamics over a fixed time interval ($t_k - n$ to t_k). The second input variable $W(t_k)$ indicates the pitching and rolling dynamics over a fixed time interval ($t_k - n$ to t_k). The output of the fuzzy inference system, namely the dynamics indicator $\text{DI}(t_k)$, is the combination of these two input dynamics measures as seen through a fuzzy inference. In the considered problem, two membership functions, "low" and "high," representing the low and high linear/angular dynamics are used for each input variable. For the purpose of computational simplicity, the triangle membership functions are used. The parameters of the input membership functions are empirically determined based on the field test data because they may vary with the vehicle vibration, the sensor installation location, and the quality of IMUs. Specifically, we use the values of $J(t_k)$ and $W(t_k)$ under the stationary and nonstationary dynamics to define the scope of the input membership functions. For the output membership functions, three triangles with full overlaps between each set and even segmentation from zero to one are used. The linguistic term "large" in the output membership functions means a higher likelihood that the vehicle is moving. A set of if-then rules for mapping the input fuzzy sets into the output fuzzy set is established by common sense reasoning and expert knowledge to the problems, e.g., the larger the values of $J(t_k)$ and $W(t_k)$, the higher the likelihood that the vehicle is moving. The designed membership functions and fuzzy rules are shown in Fig. 1 and Table II, respectively.

To complete the inference procedure and to generate the output fuzzy set, the Mamdani type fuzzy inference method with max-min composition,

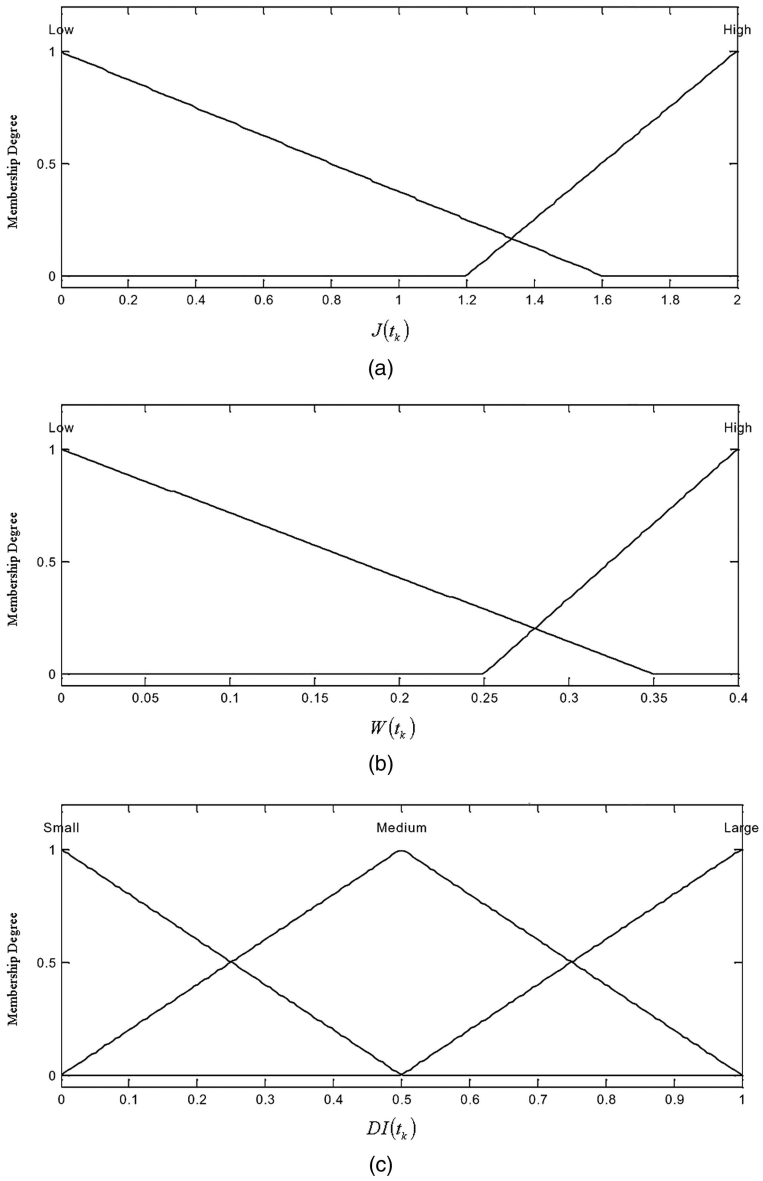

Fig. 1. (a) Membership functions used in fuzzy inference system for first input variable. (b) Membership functions used in fuzzy inference system for second input variable. (c) Membership functions used in fuzzy inference system for output variable.

which is considered as the most commonly seen fuzzy methodology, has been used [22]. The output fuzzy set is defuzzified into a crisp value using the centre of the area method. According to the designed output membership functions, the final crisp output, i.e., the dynamics indicator $\mathrm{DI}(t_k)$, is in a range between 1/6 and 5/6, and it becomes straightforward to distinguish between the stationary and nonstationary dynamics using a cutoff value of 0.5.

When the dynamics indicator $\mathrm{DI}(t_k)$ is used for stationary and nonstationary identification, there exists the detection delay because the fuzzy input variables $J(t_k)$ and $W(t_k)$ are formed by a set of data from the previous epoch to the current epoch. To overcome this problem, we define another linear dynamics parameter $\mathrm{DA}_x(t_k)$ to measure the instant forward dynamics as follows:

TABLE II
If-Then Rules used in the Fuzzy Inference System for Vehicle Dynamics Identification

R_1: If $J(t_k)$ is LOW and $W(t_k)$ is LOW then $\mathrm{DI}(t_k)$ is SMALL
R_2: If $J(t_k)$ is HIGH and $W(t_k)$ is LOW then $\mathrm{DI}(t_k)$ is MEDIUM
R_3: If $J(t_k)$ is LOW and $W(t_k)$ is HIGH then $\mathrm{DI}(t_k)$ is MEDIUM
R_4: If $J(t_k)$ is HIGH and $W(t_k)$ is HIGH then $\mathrm{DI}(t_k)$ is LARGE

$$\mathrm{DA}_x(t_k) = \sum_{t_i=t_k-p}^{t_k} |A_{Bx}(t_i) - A_{Bx}(t_k - p)| \qquad (20)$$

where p is the time lag for the computation of the acceleration difference.

When the vehicle begins to move from a stationary status, a dramatic dynamics change occurs in the

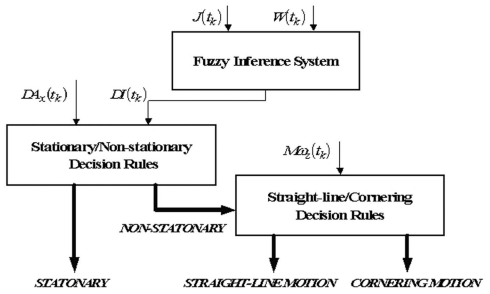

Fig. 2. Decision flow of vehicle dynamics identification system.

TABLE III
Expert Rules for Stationary/Nonstationary Identification

R_1:	When the vehicle was stationary at the last epoch: If $\mathrm{DA}_x(t_k)$ is larger than a criterion value, then the vehicle is nonstationary
R_2:	When the vehicle was nonstationary at the last epoch: If $\mathrm{DA}_x(t_k)$ is smaller than a criterion value and $\mathrm{DI}(t_k)$ is smaller than 0.5, then the vehicle is stationary

TABLE IV
Expert Rules for Straight-Line/Cornering Motion Identification

R_1:	When the vehicle was in straight-line motion at the last epoch: If $M\omega_z(t_k)$ is larger than a criterion value, then the vehicle is in cornering motion.
R_2:	When the vehicle was in cornering motion at the last epoch: If $M\omega_z(t_k)$ is smaller than a criterion value, then the vehicle is in straight-line motion.

forward direction. In this case, $\mathrm{DA}_x(t_k)$ becomes significant and can be used to instantly indicate the dynamics transition from stationary to move. Based on the conditions of $\mathrm{DI}(t_k)$ and $\mathrm{DA}_x(t_k)$, a set of if-then rules shown in Table III is constructed to distinguish the status of vehicle dynamics, either stationary or nonstationary.

When the vehicle dynamics is identified as nonstationary, the next task is to distinguish the vehicle dynamics between straight-line motion and cornering motion. Since the pitch and roll angles are generally small during the cornering motion of a land vehicle, the z-axis gyro measurement ω_{Bz} can be directly used to represent the yawing dynamics. By simple averaging of ω_{Bz} over a fixed time interval to reduce noise effects, a cornering dynamics measure can be computed as follows:

$$M\omega_z(t_k) = \frac{1}{m}\sum_{t_i=t_k-m}^{t_k} \omega_{Bz}(t_i) \tag{21}$$

where m is the size of the time window for the moving average.

Based on the conditions of $M\omega_z(t_k)$, a set of if-then rules shown in Table IV can be constructed to classify the nonstationary dynamics as straight-line motion or cornering motion. In Table III and Table IV, the if-then rules used for identifying stationary, straight-line motion, and cornering motion can be easily formulated by common sense reasoning and expert knowledge of the problems. The criterion value used in each rule is heuristically determined based on the real data and is vehicle dependent and sensitive to the installation locations of the sensors. The decision flow of the designed vehicle dynamics identification system is shown in Fig. 2.

IV. DEAD-RECKONING KALMAN FILTER DESIGN

Navigation derived from time integration of the inertial measurements based on the land vehicle motion equation experiences large error accumulation and requires an error control mechanism. The dead-reckoning or integration Kalman filter here is developed to estimate the INS sensor and navigation errors using dynamics-aided or external sensors-aided measurements. As the dynamics-derived observables are only available in velocity and attitude domain, we focus on analyzing the velocity and attitude estimation of the dynamics-aided inertial navigator for simplicity. The design of the INS dead-reckoning filter is basically the design of INS error dynamics models and measurement statistics.

A. Dynamics Model

The inertial navigation error dynamics models are derived from the land vehicle motion mode using the perturbation technique of (1)–(6). The inertial sensor errors including biases and noises are modeled by a random walk process in the Kalman filter. Including navigation and sensor errors, the final system error models are constructed as shown in (22). It should be noted that the error model doesn't include the y-axis accelerometer error because it is unobservable and has no impact on the velocity and attitude estimation. The three-axis gyro biases are considered as already removed from the measurements using the averaging stationary gyro measurements after each stop of the vehicle.

$$\underbrace{\begin{bmatrix} \delta\dot{V}_f \\ \delta\dot{\phi} \\ \delta\dot{\theta} \\ \delta\dot{\psi} \\ \dot{b}_{A_{Bx}} \end{bmatrix}}_{\dot{\mathbf{x}}} = \underbrace{\begin{bmatrix} 0 & 0 & -g\cos\theta & 0 & 1 \\ 0 & f_{\phi\phi} & f_{\phi\theta} & 0 & 0 \\ 0 & f_{\theta\phi} & 0 & 0 & 0 \\ 0 & f_{\psi\phi} & f_{\psi\theta} & 0 & 0 \\ 0 & 0 & 0 & 0 & 0 \end{bmatrix}}_{\mathbf{F}} \underbrace{\begin{bmatrix} \delta V_f \\ \delta\phi \\ \delta\theta \\ \delta\psi \\ b_{A_{Bx}} \end{bmatrix}}_{\mathbf{x}}$$
$$+ \underbrace{\begin{bmatrix} 1 & 0 & 0 & 0 & 0 \\ 0 & 1 & \sin\phi\tan\theta & \cos\phi\tan\theta & 0 \\ 0 & 0 & \cos\phi & -\sin\phi & 0 \\ 0 & 0 & \sin\phi\sec\theta & \cos\phi\sec\theta & 0 \\ 0 & 0 & 0 & 0 & 1 \end{bmatrix}}_{\mathbf{G}} \underbrace{\begin{bmatrix} w_{A_{Bx}} \\ w_{\omega_{Bx}} \\ w_{\omega_{By}} \\ w_{\omega_{Bz}} \\ w_b \end{bmatrix}}_{\mathbf{u}} \tag{22}$$

where δV_f is the forward velocity error; $\delta\phi$, $\delta\theta$, $\delta\psi$ are the roll, pitch, and yaw errors; $b_{A_{Bx}}$ is the x-axis accelerometer bias; $w_{A_{Bx}}$ is the x-axis accelerometer noise; $w_{\omega_{Bx}}$, $w_{\omega_{By}}$, $w_{\omega_{Bz}}$ are the gyro noises on each axis; w_b is the driving noise for the accelerometer bias; and

$$
\begin{aligned}
f_{\phi\phi} &= \cos\phi\tan\theta\omega_{By} - \sin\phi\tan\theta\omega_{Bz};\\
f_{\phi\theta} &= \sin\phi\sec^2\theta\omega_{By} + \cos\phi\sec^2\theta\omega_{Bz};\\
f_{\theta\phi} &= -\sin\phi\omega_{By} - \cos\phi\omega_{Bz};\\
f_{\psi\phi} &= \cos\phi\sec\theta\omega_{By} - \sin\phi\sec\theta\omega_{Bz};\\
f_{\psi\theta} &= \sin\phi\sec\theta\tan\theta\omega_{By} + \cos\phi\sec\theta\tan\theta\omega_{Bz}.
\end{aligned}
$$

The spectral density matrix of the input white noise is given by

$$\mathbf{Q}(t) = \mathrm{diag}(q_{A_{Bx}} q_{\omega_{Bx}} q_{\omega_{By}} q_{\omega_{Bz}} q_b) \tag{23}$$

where $q_{A_{Bx}}$ is the spectral density of the x-axis accelerometer noise; $q_{\omega_{Bx}}$, $q_{\omega_{By}}$, $q_{\omega_{Bz}}$ are the spectral densities of the gyro noises on each axis; q_b is the spectral density of the x-axis accelerometer bias.

The spectral density of the accelerometer and gyro noises can be estimated based on the standard deviation over a short period of static measurements or obtained from the manufacturer's specifications. The variation of the accelerometer bias can be calculated based on an analysis of the Allan variance over a long period of static data or obtained from the manufacturer's specifications (IEEE, Standard 952-1997). In real applications during dynamic maneuvers, however, the sensor noises and bias variations are strongly coupled with the vibration, dithering, dynamics, and environment effects, especially for low-cost MEMS IMUs. To take these effects into account, a larger spectral density of the input noise should be used, and in this paper they are determined empirically based on field test data.

B. Measurement Model

Following the dynamics-derived measurements summarized in Table I, the corresponding measurement models for stationary, straight-line motion and cornering motion are discussed separately.

When the vehicle is stationary, a direct estimation of the vehicle velocity and attitude information becomes feasible. In this mode, the measurement model can be formed as follows:

$$
\underbrace{\begin{bmatrix} V_f - 0 \\ \phi - \phi^A \\ \theta - \theta^A \\ \psi - \psi^P \end{bmatrix}}_{\mathbf{z}} = \underbrace{\begin{bmatrix} 1 & 0 & 0 & 0 & 0 \\ 0 & 1 & 0 & 0 & 0 \\ 0 & 0 & 1 & 0 & 0 \\ 0 & 0 & 0 & 1 & 0 \end{bmatrix}}_{\mathbf{H}} \underbrace{\begin{bmatrix} \delta V_f \\ \delta\phi \\ \delta\theta \\ \delta\psi \\ b_{A_{Bx}} \end{bmatrix}}_{\mathbf{x}} + \underbrace{\begin{bmatrix} v_{v_f^{\mathrm{ZUPT}}} \\ v_{\phi^A} \\ v_{\theta^A} \\ v_{\psi^P} \end{bmatrix}}_{\mathbf{v}} \tag{24}
$$

where ψ^P is the yaw angle estimated by the Kalman filter at the previous epoch; ϕ^A and θ^A are the roll and pitch angles computed using accelerometer measurements after the bias and noise are removed; and $v_{v_f^{\mathrm{ZUPT}}}$, v_{ϕ^A}, v_{θ^A}, and v_{ψ^P} represent the measurement noises for ZUPT, the accelerometer-derived roll and pitch, and the filter-derived yaw at the previous epoch, respectively. The covariance matrix of the measurement noise is given by

$$\mathbf{R} = \mathrm{diag}(\sigma^2_{\delta V_f^{\mathrm{ZUPT}}} \sigma^2_{\delta\phi^A} \sigma^2_{\delta\theta^A} \sigma^2_{\delta\psi^P}) \tag{25}$$

where $\sigma_{\delta V_f^{\mathrm{ZUPT}}}$ is the standard deviation of the ZUPT error; $\sigma_{\delta\phi^A}$ and $\sigma_{\delta\theta^A}$ are the standard deviations of the accelerometer-derived roll and pitch errors; and $\sigma_{\delta\psi^P}$ is the standard deviation of the filter-derived yaw error at the previous epoch.

Since the vehicle has zero velocity and constant heading during a stationary period, we can assign a very small value to $\sigma_{\delta V_f^{\mathrm{ZUPT}}}$. In order to constrain the heading estimate to the previously derived heading during the stationary period, we also assign a very small value to $\sigma_{\delta\psi^P}$. For the determination of $\sigma_{\delta\phi^A}$ and $\sigma_{\delta\theta^A}$, they are assigned small values of 0.2 deg because the accelerometer-derived roll and pitch after bias compensation are very accurate compared with the gyro-derived roll and pitch which have large drift errors.

When the vehicle is moving straight, the accelerometer-derived roll is the only dynamics-derived measurement available to update the velocity and attitude filter. The measurement model is formed as follows:

$$
\underbrace{[\phi - \phi^A]}_{\mathbf{z}} = \underbrace{[0 \quad 1 \quad 0 \quad 0 \quad 0]}_{\mathbf{H}} \underbrace{\begin{bmatrix} \delta V_f \\ \delta\phi \\ \delta\theta \\ \delta\psi \\ b_{A_{Bx}} \end{bmatrix}}_{\mathbf{x}} + \underbrace{[v_{\phi^A}]}_{\mathbf{v}}. \tag{26}
$$

The covariance matrix of the measurement noise is given by

$$\mathbf{R} = \sigma^2_{\delta\phi^A} \tag{27}$$

Similarly, we assign a small value of 0.2 deg to $\sigma_{\delta\phi^A}$ because the accelerometer-derived roll after bias compensation is accurate enough to correct the drift errors of the gyro-derived roll.

When the vehicle is making a turn, the forward velocity is the only dynamics-derived measurement available to update the velocity and attitude filter. The measurement model is formed as follows:

$$
\underbrace{[V_f - V_f^C]}_{\mathbf{z}} = \underbrace{[1 \quad 0 \quad 0 \quad 0 \quad 0]}_{\mathbf{H}} \underbrace{\begin{bmatrix} \delta V_f \\ \delta\phi \\ \delta\theta \\ \delta\psi \\ b_{A_{Bx}} \end{bmatrix}}_{\mathbf{x}} + \underbrace{[v_{v_f^C}]}_{\mathbf{v}} \tag{28}
$$

where V_f^C is the dynamics-derived forward velocity after the bias and noise have been removed, and $v_{v_f^C}$ represents the measurement noise of V_f^C. The covariance matrix of the measurement noise is given by

$$\mathbf{R} = \sigma^2_{\delta V_f^C} \tag{29}$$

where $\sigma_{\delta V_f^C}$ is the standard deviation of the dynamics-derived forward velocity error.

As stated previously, the accuracy of the dynamics-derived forward velocity is mainly dependent on the quality of the y-axis accelerometer and the z-axis gyro measurements as well as the vibration and road ruggedness effects during the cornering motion. Therefore, $\sigma_{\delta V_f^C}$ is defined empirically according to the field test data.

It should be noted that the x-axis and y-axis accelerometer biases must be determined first in order to correctly derive the above dynamics-based observations. As shown in (22), the x-axis accelerometer bias is already modeled in the filter and can be estimated when the velocity updates from an external sensor such as GPS are available. For the y-axis accelerometer bias estimation, in this paper we have developed a statistical approach based on the forward velocity computation model described in (15). Arranging the y-axis acceleration term to the left-hand side of the equation, we rewrite (15) as follows:

$$A_{By} = \omega_{Bz} V_f - g \sin\phi \cos\theta. \tag{30}$$

As mentioned previously, the bias term in the z-axis gyro measurement (ω_{Bz}) can be removed directly once the vehicle is stationary. The corrected V_f, ϕ, and θ can be estimated by the velocity and attitude Kalman filter when external sensor aids are available. After the Kalman filter reaches a steady-state condition, more accurate estimates can be obtained as well. Therefore, applying these corrected terms in (30), we can calculate the unbiased y-axis body acceleration. Furthermore, taking the difference between this unbiased acceleration and the y-axis accelerometer measurement, we can compute the acceleration error that is mainly contributed by the accelerometer bias and noise as well as the noises from ω_{Bz}, V_f, ϕ, and θ. A simple approach to resolve the accelerometer bias is to remove the noise effects by averaging a set of data and use this mean value as the constant part of the y-axis accelerometer bias. The estimate of the y-axis accelerometer bias $\hat{b}_{A_{By}}$ using the statistical approach is given by the following equation:

$$\hat{b}_{A_{By}} = \frac{1}{M}\sum_{t_k=1}^{M} A_{By}(t_k) - \bar{\omega}_{Bz}(t_k)\hat{V}_f(t_k) + g\sin\hat{\phi}(t_k)\cos\hat{\theta}(t_k) \tag{31}$$

where A_{By} is the y-axis accelerometer measurement; $\bar{\omega}_{Bz}$ is the z-axis bias-removed gyro measurement; $\hat{V}_f$, $\hat{\phi}$, and $\hat{\theta}$ are the estimates of the velocity, roll, and pitch given by the Kalman filter; and M is the number of data used for averaging process.

In order to estimate the y-axis accelerometer bias more accurately, only the data obtained during the cornering motion and after the convergence of the Kalman filter are used for bias computation. This is because A_{By} and $\bar{\omega}_{Bz}$ have a higher signal-to-noise ratio during the cornering motion and $\hat{V}_f$, $\hat{\phi}$, and $\hat{\theta}$ have better accuracy after the convergence of the Kalman filter.

It should be noted that the accuracy of some dynamics-derived observations, including stationary tilt, straight-line roll, and cornering velocity are correlated with the inertial sensor biases and the estimated pitch and roll as shown in (12), (13), and (14). This will violate the assumption of the uncorrelated property between measurement noise and process noise in the Kalman filter if using these dynamics-derived observations to estimate the inertial sensor biases and tilt. To avoid this correlation violation, we disable the accelerometer bias estimation in the dynamics-aided INS mode (during outage of external sensor aids). The accelerometer bias is estimated when the external sensor aids are available and then used to correct dynamics-derived observables during the followed outage of the external sensor. This strategy not only ensures the stability of the bias estimation but also avoids the dynamics-derived measurements to be correlated with the Kalman filter system state, i.e., the x-axis accelerometer bias. As the pitch and roll angles are generally small in land vehicle environments, the correlation between the dynamics-derived measurements and the tilt errors is not significant. Compared with the unaided INS navigation which has large error drift, it is worthwhile to use these dynamics-derived measurements to bound the INS velocity and tilt errors even though they are slightly correlated.

V. TEST RESULTS AND DISCUSSIONS

A van test has been conducted at the University of Calgary Parking Lot to evaluate the proposed dynamics-aided inertial navigation algorithm. A test trajectory with eight cornering shapes and four virtual stop signs was chosen to allow diverse driving dynamics as shown in Fig. 3. Ten data collection runs on the selected trajectory were performed, each starting in stationary for about 1 min and followed by about 3 min of driving and a 10 s stop at each stop point. The test system contains an Xsens MT9 MEMS IMU and a SiRF Star II Xtrac high sensitivity GPS receiver. The reference solutions are provided by a highly precise INS/GPS integration system consisting

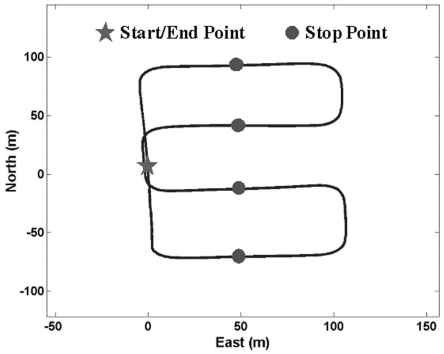

Fig. 3. Open area test trajectory.

of a tactical-grade Honeywell HG1700 IMU and a high-performance NovAtel OEM4 dual frequency GPS receiver postprocessed by using P3-INS software. The P3-INS software is developed by the positioning and mobile information system (PMIS) group in the Department of Geomatics Engineering at the University of Calgary. It integrates precise point positioning (PPP) with inertial technologies to provide globally attainable accuracy for position at the centimeter to decimeter level and for attitude at the several arcmin level [23].

Two-step test scenarios are applied to evaluate the proposed dynamics-aided inertial navigation algorithm. In the first step, the filter uses only a GPS update to estimate the accelerometer biases for each run. In the second step, we artificially disuse GPS update and only use dynamics-derived measurements that have been corrected using the accelerometer biases obtained from the previous run to update the filter in the current run. Thus, a total of nine-run tests are assessed for the standalone dynamics-aided inertial navigation performance. The accuracies of vehicle dynamics identification and dynamics-derived measurements are evaluated first, followed by the performance assessment of a standalone dynamics-aided INS.

Fig. 4 shows the results of the vehicle dynamics identification for a sample run 7. By comparing the identified motion type with the reference velocity and yaw rate, we verify that the vehicle motion types including the stationary, straight-line motion, and cornering motion have been correctly identified. It should be noted that there exists a straight-line motion between the sixth and the seventh cornering motions that was not identified by the designed fuzzy expert system. This is an expected and acceptable condition since the periods of the straight-line motion between the two continuous cornering motions are too short to be recognizable by the designed fuzzy expert system. Similar identification results for other runs have been also obtained but not shown here.

Figs. 5–7 show the dynamics-derived and reference pitch, roll, and velocity using the data collected in the same sample run. As shown in Figs. 5 and 6, the dynamics-derived pitch and roll are considerably accurate with very small bias with the reference. This implies that good bias estimation accuracy has been obtained by the INS/GPS system in the previous run. Due to the approximation errors induced by sideslips or vibrations, the dynamics-derived roll in the straight-line motion mode has relatively larger errors than the dynamics-derived roll in the stationary mode. For the cornering motion mode, as shown in Fig. 7, the dynamics-derived velocities are close to the reference velocities so that they can be used to correct the stand-alone INS velocities and reduce the error drift. The errors of all dynamics-derived observations are shown in Fig. 8 which demonstrates the error characteristics we have described above. It should be noted that there exist some oscillatory errors in the stationary pitch and roll at the beginning of the stationary period. This is because the stationary pitch and roll are not smoothed at the beginning of the stationary period due to the lack of samples for moving average. As the samples for the moving average increase, this type of error will be filtered, and the stationary pitch and roll remain steady.

Table V summarizes the accuracy of the dynamics-derived observations given by the nine-run data. The average mean of the dynamic-derived pitch and roll errors (about 0.16 deg) represents the unidentified accelerometer bias (about 0.025 m/s^2)

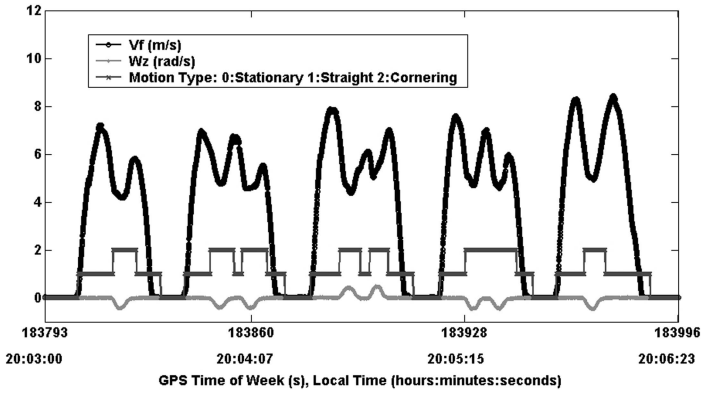

Fig. 4. Results of vehicle dynamics identification.

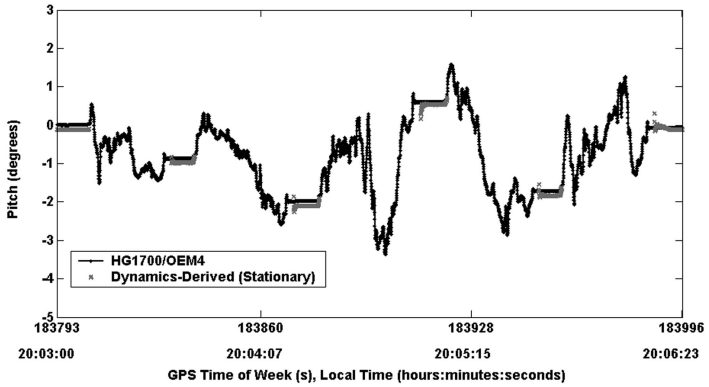

Fig. 5. Dynamics-derived pitch observations.

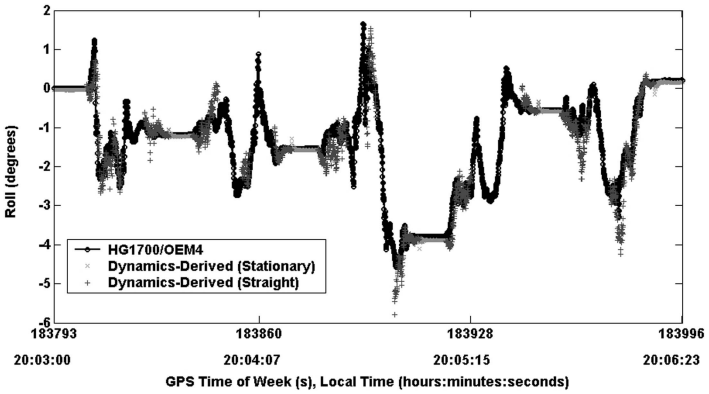

Fig. 6. Dynamics-derived roll observations.

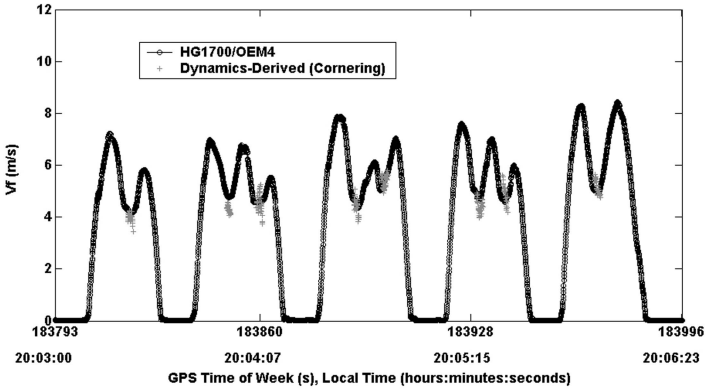

Fig. 7. Dynamics-derived velocity observations.

given by the INS/GPS system. We observed that in each test the rms error of the dynamic-derived stationary pitch and roll is almost identical to the absolute value of the mean error. This is because the stationary pitch and roll error is mainly due to the unidentified accelerometer bias after the noise effects have been removed by a moving average. Due to the approximation errors induced by sideslips or vibrations, the rms error of the dynamics-derived roll in the straight-line motion mode is larger than the rms error of the stationary roll. For the cornering motion rms mode, the accuracy of the dynamics-derived velocity is about 0.45 m/s and considerably stable for each test. Compared to the stand-alone INS navigation solutions, the dynamics-derived observations are accurate enough to provide pitch, roll and velocity corrections.

The pitch, roll, and heading estimates of the dynamics-aided INS for the sample run 7 are shown in Figs. 9–11. To demonstrate the benefits of the dynamics aids, the unaided stand-alone INS solution is also displayed. In the unaided mode, no dynamics-derived observations are used to update the Kalman filter, and thus the filter works in a full prediction mode. As shown in Figs. 9 and 10, the error of the dynamics-aided pitch and roll are

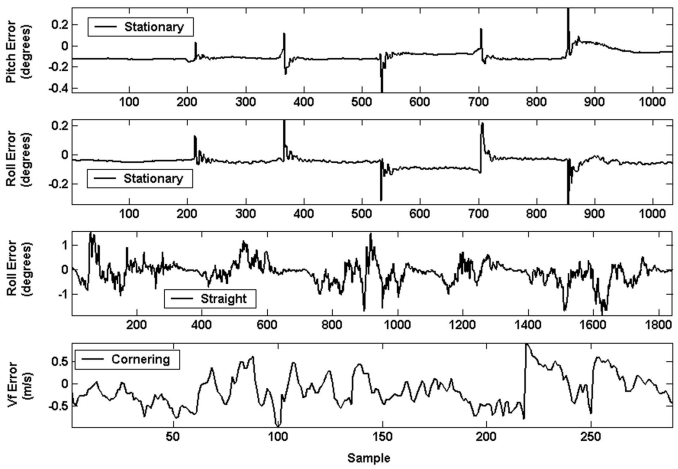

Fig. 8. Errors of dynamics-derived observations.

TABLE V
Dynamics-Derived Observation Accuracy

	Stationary Pitch Error (deg)		Stationary Roll Error (deg)		Straight-Line Roll Error (deg)		Cornering Velocity Error (m/s)	
Test No.	Mean	rms	Mean	rms	Mean	rms	Mean	rms
2	−0.26	0.27	0.05	0.10	−0.01	0.46	−0.20	0.50
3	−0.13	0.14	0.16	0.17	0.15	0.44	−0.27	0.51
4	0.16	0.16	0.38	0.38	0.31	0.54	−0.18	0.42
5	0.04	0.06	0.01	0.06	0.01	0.45	−0.20	0.46
6	−0.03	0.04	−0.42	0.42	−0.45	0.68	−0.12	0.48
7*	−0.10	0.11	−0.05	0.06	−0.11	0.46	−0.13	0.38
8	−0.18	0.18	−0.20	0.20	−0.23	0.52	−0.25	0.42
9	−0.35	0.35	0.18	0.18	0.16	0.44	−0.19	0.42
10	−0.25	0.25	0.03	0.05	−0.05	0.42	−0.26	0.43
Average	0.17**	0.17	0.16**	0.18	0.16**	0.49	0.20**	0.45

Note: *This is the sample run of test whose results are shown in Figs. 5–8.
**This value is calculated by averaging the absolute value of each run of test.

bounded and well controlled, but the unaided pitch and roll have large error drifts. The dynamics-aided pitch estimates during the stationary periods as well as the roll estimates during the stationary and the straight-line motion periods are almost identical to the dynamics-derived pitch and roll shown in Figs. 5 and 6, respectively. This is because the pitch and roll states in the INS Kalman filter are directly observable from the dynamics-derived measurements and their covariances are very small. For the periods when the dynamics-derived pitch and roll updates are unavailable, the performance of the dynamics-aided tilt estimates degrades with time. The performance degradation is mainly dependent on the quality of the inertial sensors and vehicle dynamics. Comparing Fig. 9 with Fig. 10, we observed that the dynamics-aided roll estimates are more accurate than the pitch due to the availability of the roll measurement updates during the straight-line motion periods. For the heading performance, an examination of the heading estimates at the end of the test indicates that the error drifts of the dynamics-aided and unaided solutions are about 1 and 2 deg, respectively. The improvement in heading is not as significant as the improvement in the tilt. This is because for the dynamics-aided INS, only the constant heading constraint during the stationary periods is available to control the heading error drift while the absolute tilt measurement updates are more frequently available to reduce the tilt error drift. In summary, the aiding from the vehicle dynamics knowledge enables the stand-alone MEMS INS to provide bounded tilt and heading solutions with reduced error drift rates.

Table VI presents the accuracy of the stand-alone dynamics-aided attitude obtained from the nine-run tests. As shown, the average rms error is about 0.8 deg for the pitch estimate, about 0.5 deg for the roll estimate and about 1.5 deg for the heading estimate. The attitude accuracy of the dynamics-aided INS is dependent on the availability and the quality of the dynamics-derived attitude updates, i.e., the periods of the stationary and straight-line motion as well as the accuracy of the preestimated accelerometer biases.

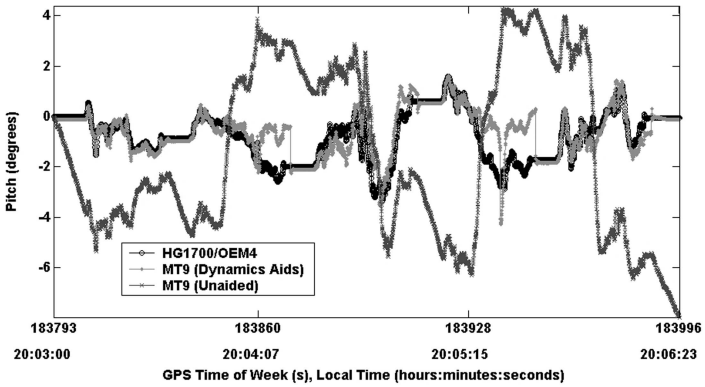

Fig. 9. Estimation results of pitch (stand-alone INS with dynamics aid).

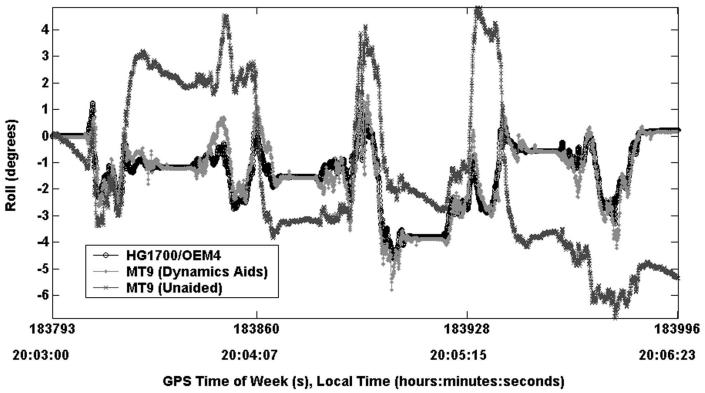

Fig. 10. Estimation results of roll (stand-alone INS with dynamics aid).

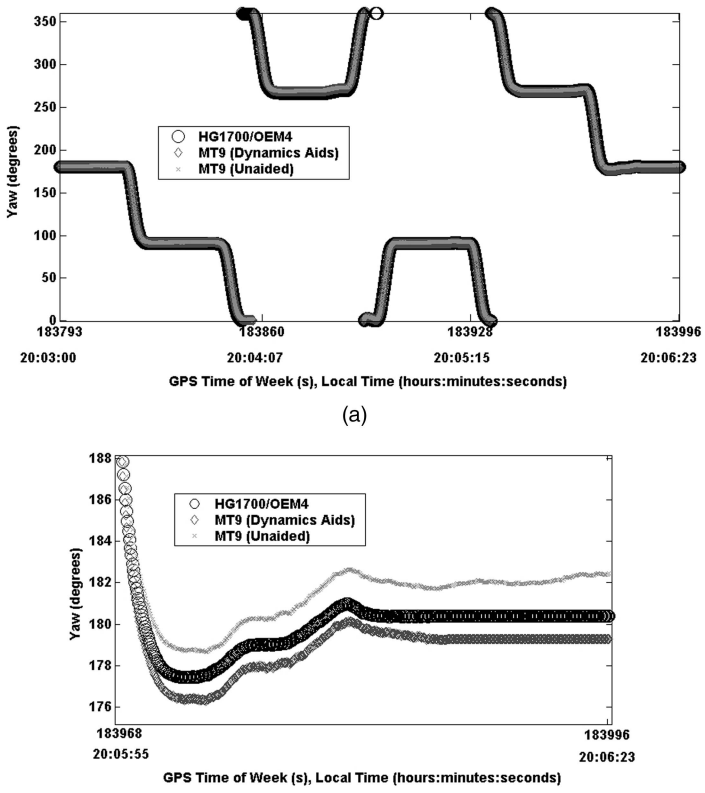

Fig. 11. (a) Estimation results of heading (stand-alone INS with dynamics aid). (b) Estimation results of heading at end of test (stand-alone INS with dynamics aid).

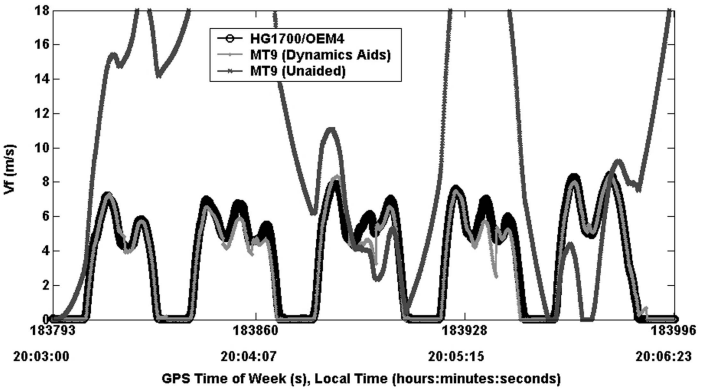

Fig. 12. Estimation results of velocity (stand-alone INS with dynamics aid).

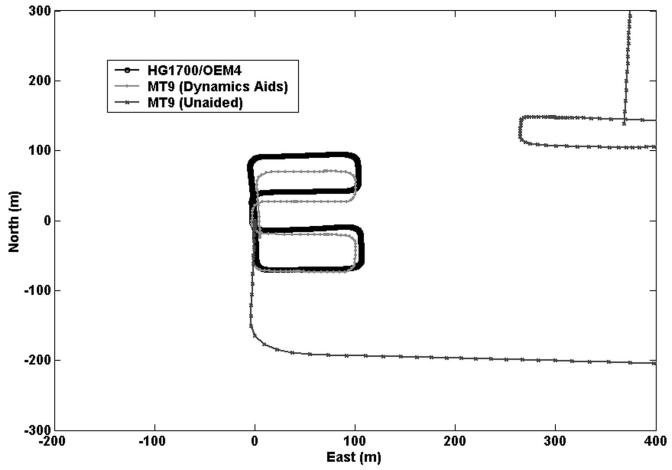

Fig. 13. Estimation results of position (stand-alone INS with dynamics aid).

TABLE VI
Attitude Estimation Accuracy (Stand-Alone INS with Dynamics Aid)

	Pitch Error (deg)		Roll Error (deg)		Heading Error (deg)	
Test No.	Mean	rms	Mean	rms	Mean	rms
2	0.18	0.71	0.10	0.54	1.17	1.70
3	0.41	1.11	0.29	0.58	−0.09	1.06
4	0.48	0.85	0.36	0.59	0.07	1.23
5	0.39	1.00	−0.01	0.58	−0.68	1.48
6	0.06	0.53	−0.38	0.60	0.95	1.10
7*	0.19	0.67	−0.01	0.45	0.62	1.36
8	−0.28	0.82	−0.14	0.48	2.30	2.47
9	−0.09	0.51	0.30	0.56	1.91	2.10
10	0.18	0.63	0.06	0.46	−0.62	1.19
Average	0.25**	0.76	0.18**	0.54	0.93**	1.52

Note: *This is the sample run of test whose results are shown in Figs. 9–11.
**This value is calculated by averaging the absolute value of each run of test.

Figs. 12 and 13 show the velocity and position solutions obtained from the dynamics-aided and unaided MEMS INS and the geo-reference system from the sample run 7, respectively. As shown in Fig. 12, the unaided velocity has large drifted errors and cannot be used for navigation while the dynamics-aided velocity error is well bounded by the ZUPTs and cornering velocity updates. During the straight-line motion, the dynamics-aided velocity error increases with time, and the error growth rate is mainly dependent on the pitch accuracy. As to the position performance, since position is directly computed by the velocity and attitude information based on dead-reckoning equations, the position error will accumulate with the course of time and is proportional to the velocity and attitude errors.

TABLE VII
Velocity and Position Estimation Accuracy (Stand-Alone INS with Dynamics Aid)

Test No.	Velocity Error (m/s)		North Position Error (m)		East Position Error (m)		Horizontal Position Error (m)	
	Mean	rms	|Max|	rms	|Max|	rms	|Max|	rms
2	−0.37	0.62	18.72	7.41	16.83	7.62	20.18	10.63
3	−0.38	0.75	18.37	8.51	25.36	13.14	29.19	15.65
4	−0.29	0.56	19.90	10.80	12.49	6.23	20.65	12.46
5	−0.30	0.82	33.15	19.22	32.05	16.78	43.93	25.51
6	−0.14	0.47	20.73	9.84	19.04	9.81	23.32	13.89
7*	−0.21	0.52	26.75	15.00	11.15	5.19	26.75	15.87
8	0.05	0.92	40.82	15.00	21.92	12.55	46.33	19.56
9	−0.22	0.56	22.39	11.53	19.95	9.78	26.55	15.12
10	−0.44	0.70	28.16	15.29	18.84	8.64	30.37	17.57
Average	0.27**	0.66	25.44	12.51	19.74	9.97	29.70	16.25

Note: *This is the sample run of test whose results are shown in Figs. 12 and 13.
**This value is calculated by averaging the absolute value of each run of test.

As shown in Fig. 13, the dynamics-aided INS positions still remain on the track while the unaided solutions have drifted away from the track at the several hundred meter level. The dynamics-aided INS horizontal position error during a GPS outage of about 3 min has been controlled to be within 27 m.

Table VII further summaries the dynamics-aided velocity and position accuracy obtained from the nine-run data. We found that the East position accuracy is better than the North because of the frequent stops available during the Eastward/Westward driving. In summary, during about 3 min stand-alone navigation, the average rms error of 0.66 m/s for velocity and of 16.25 m for horizontal position are obtainable while the average maximum horizontal position error has been kept within 30 m. The achieved performance is much better than the performance supplied by the manufacturer specifications, which demonstrates the effectiveness of the developed dynamics-knowledge-aiding method for low-cost MEMS INS navigation during primary aiding sensor outage.

VI. CONCLUSIONS

This paper has developed a dynamics-aiding method to improve the low-cost MEMS INS/GPS navigation over long GPS outages. The development of dynamic-dependent observables and vehicle dynamics identification system as well as the integration of dynamics-aided data with the INS/GPS Kalman filter have been presented. The field tests have shown position accuracy of around 15 m with GPS outages of 3 min long using the developed dynamics-aiding method, but the position error of the unaided system will be as large as 100 m. The developed dynamic aiding method is self-contained and requires no additional sensors. It is particularly suitable for land vehicle navigation in urban canyon with severe GPS signal degradation and frequent vehicle stops and turning dynamics.

REFERENCES

[1] Wei, M. and Schwarz, K. P.
Testing a decentralized filter for GPS/INS integration.
In *Proceedings of the IEEE PLANS 1990*, Las Vegas, NV, Mar. 1990, 429–435.

[2] Cannon, M. E.
Airborne GPS/INS with an application to aerotriangulation.
Ph.D. dissertation, Dept. of Geomatics Engineering, University of Calgary, AB, Canada, 1991.

[3] Scherzinger, B. M.
Precise robust positioning with inertial/GPS RTK.
In *Proceedings of the Institute of Navigation GPS 2000*, Salt Lake City, UT, Sept. 2000, 155–162.

[4] Salychev, O., Voronov, V. V., Cannon, M. E., Nayak, R. A., and Lachapelle, G.
Low cost INS/GPS integration: Concepts and testing.
In *Proceedings of the Institute of Navigation* (NTM 2000), Anaheim, CA, Jan. 2000, 98–105.

[5] Brown, A. and Lu, Y.
Performance test results on an integrated GPS/MEMS inertial navigation package.
In *Proceedings of the Institute of Navigation* (GNSS 2004), Long Beach, CA, Sept. 2004, 825–832.

[6] Jaffe, R., Bonomi, S., and Madni, A. M.
Miniature MEMS quartz INS/GPS description and performance attributes.
In *Proceedings of the Institute of Navigation* (GNSS 2004), Long Beach, CA, Sept. 2004, 852–863.

[7] Ibrahim, F., Al-Holou, N., Pilutii, T., and Tascillo, A.
DGPS/INS integration using linear neurons.
In *Proceedings of the Institute of Navigation* (GPS 2000), Salt Lake City, UT, Sept. 2000, 2455–2463.

[8] Chiang, K. W.
INS/GPS integration using neural networks for land vehicular navigation applications.
Ph.D. dissertation, Dept. Geomatics Engineering, University of Calgary, AB, Canada, 2004.

[9] El-Sheimy, N., Walid, A-H., and Lachapelle, G.
An adaptive neuro-fuzzy model for bridging GPS outages in MEMS-IMU/GPS land vehicle navigation.
In *Proceedings of the Institute of Navigation* (GNSS 2004), Long Beach, CA, Sept. 2004, 1088–1095.

[10] Haykin, S.
Neural Networks: A Comprehensive Foundation.
Upper Saddle River, NJ: Prentice-Hall, 1999.

[11] Salychev, O.
Inertial Systems in Navigation and Geophysics.
Moscow, Russia: Bauman MSTU Press, 1998.

[12] Brandt, A., and Gardner, J. F.
Constrained navigation algorithms for strapdown inertial navigation systems with reduced set of sensors.
In *Proceedings of the American Control Conference*, Philadelphia, PA, June 1998, 1848–1852.

[13] Dissanayake, G., Sukkarieh, S., Nebot, E., and Durrant-Whyte, H.
The aiding of a low-cost strapdown inertial measurement unit using vehicle model constraints for land vehicle applications.
IEEE Transactions on Robotics and Automation, **17**, 5 (Oct. 2001), 731–747.

[14] Shin, E-H.
Estimation techniques for low-cost inertial navigation.
Ph.D. dissertation, Dept. of Geomatics Engineering, University of Calgary, AB, Canada, 2005.

[15] Collin, J., Käppi, J., and Saarinen, J.
Unaided MEMS-based INS application in a vehicular environment.
In *Proceedings of the Institute of Navigation* (GPS 2001), Salt Lake City, UT, Sept. 2001, 1343–1348.

[16] Ojeda, L. and Borenstein, J.
FLEXnav: fuzzy logic expert rule-based position estimation for mobile robots on rugged terrain.
In *Proceedings of the 2002 IEEE International Conference on Robotics and Automation*, Washington, D.C., May 2002, 317–322.

[17] Wang, J-H. and Gao, Y.
Fuzzy logic expert rule-based multi-sensor data fusion for land vehicle attitude estimation.
In *Proceedings of the 19th International CODATA Conference*, Berlin, Germany, Nov. 2004.

[18] Wang, J-H., Gao, Y., and Zhang, Y.
An intelligent MEMS IMU-based land vehicle navigation system enhanced by dynamics knowledge.
In *Proceedings of the Institute of Navigation* (AM 2005), Cambridge, MA, June 2005, 1141–1150.

[19] Sukkarieh, S.
Low cost, high integrity, aided inertial navigation systems for autonomous land vehicles.
Ph.D. dissertation, Australian Centre for Field Robotics, Dept. of Mechanical and Mechatronic Engineering, University of Sydney, Sydney, Australia, 2000.

[20] Kandel, A. (Ed.)
Fuzzy Expert Systems.
Boca Raton, FL: CRC Press, 1992.

[21] Jang, J-S. R., Sun, C-T., and Mizutani, E.
Neuro-Fuzzy and Soft Computing.
Upper Saddle River, NJ: Prentice-Hall, 1997.

[22] Mamdani, E. H. and Assilian, S.
An experiment in linguistic synthesis with fuzzy logic controller.
International Journal of Man-Machine Studies, **7**, 1 (1975), 1–13.

[23] Zhang, Y. and Gao, Y.
Performance analysis of a tightly coupled Kalman filter for the integration of undifferenced GPS and inertial data.
In *Proceedings of the Institute of Navigation* (NTM 2005), San Diego, CA, Jan. 2005, 270–275.

Jau-Hsiung Wang received his Ph.D. in geomatics engineering in 2006 from The University of Calgary, Calgary, Alberta, Canada. Prior to that, he received a B.Sc. in mechanical engineering in 1995 from National Taiwan University of Science and Technology, Taipei, Taiwan, and an M.Sc. in applied mechanics in 1997 from National Taiwan University, Taipei, Taiwan.

He is currently a navigation analyst in the Advanced Technology Group at Applanix, a Trimble Company, Richmond Hill, Ontario, Canada. His research focuses on the development of inertial aided satellite navigation systems and algorithms.

Dr. Wang is the member of the International Association of Chinese Professionals in Global Positioning Systems. He is the recipient of the U.S. Institute of Navigation GNSS 2004 Best Student Paper Award, and the 2004 Sangster Award by the Canadian National Committee for CODATA.

Yang Gao received his Ph.D. in satellite geodesy in 1993 from The University of Calgary, Calgary, Alberta, Canada. Prior to that, he received a B.Sc. in 1982 and an M.Sc. in 1985 from Wuhan University, Wuhan, China.

He is currently a professor in the Department of Geomatics Engineering at The University of Calgary, Calgary, Alberta, Canada. He is the Luojia Chair Professor at Wuhan University. His research focuses on the development of novel methods and algorithms using satellite-based navigation systems such as Global Positioning System (GPS) and their integration with other enabling sensors.

Dr. Gao has published over 100 technical papers in the field of satellite positioning and navigation. He is a member of the U.S. Institute of Navigation, the Canadian Institute of Geomatics, and the past president of the International Association of Chinese Professionals in Global Positioning Systems. He is the Chairman of Sub-Commission 4.5 “Next Generation RTK” in the International Association of Geodesy (IAG).